

The electrical conductivity of cubic $(\text{In}_{1-x}\text{Ga}_x)_2\text{O}_3$ films ($x \leq 0.18$): Native point defects, Sn-doping, and the surface electron accumulation layer

Alexandra Papadogianni,¹ Takahiro Nagata,² and Oliver Bierwagen¹

¹*Paul-Drude-Institut für Festkörperelektronik, Leibniz-Institut im Forschungsverbund Berlin e.V., Hausvogteiplatz 5–7, D–10117 Berlin, Germany*

²*National Institute for Materials Science, 1-1 Namiki Tsukuba, 305-0044 Ibaraki, Japan*

(Dated: September 28, 2021)

The alloying of the group-III transparent semiconducting sesquioxides In_2O_3 and Ga_2O_3 can lead to a modulation of the properties of the parent compounds, e.g., the shallow- and deep-donor character of the oxygen vacancy or the presence and absence of a surface electron accumulation layer, respectively. In this work, we investigate the effect of alloying on the electron transport properties of unintentionally-doped single-crystalline and textured bixbyite $(\text{In}_{1-x}\text{Ga}_x)_2\text{O}_3$ thin films annealed in oxygen and vacuum with Ga contents up to $x = 0.18$. Hall effect measurements demonstrate a surprising increase in electron density due to native defects with added Ga. This increase may be related to the incorporation of Ga-interstitials or oxygen vacancies induced by Ga-related unit-cell distortions. A combined investigation based on hard and soft x-ray photoelectron spectroscopy measurements demonstrates the existence of the surface electron accumulation layer for all alloy films and, hence, no depletion up to $x = 0.18$. Finally, we additionally demonstrate a single-crystalline $(\text{In}_{0.92}\text{Ga}_{0.08})_2\text{O}_3:\text{Sn}$ film, as a possible transparent conductive oxide with a wider band gap than that of (Sn-doped) In_2O_3 .

I. INTRODUCTION

In_2O_3 and Ga_2O_3 are transparent semiconducting materials widely studied for implementation in devices.

On the one hand, In_2O_3 is typically cubic bixbyite¹ and has an optically forbidden direct band gap found to be 2.7–2.9 eV, with strong optical absorption occurring from valence bands nearly 1 eV below the valence band maximum (VBM).^{2–4} This property renders In_2O_3 transparent in the visible range of the electromagnetic spectrum and is—remarkably—combined with high electrical conductivity. In_2O_3 exhibits inherent *n*-type conductivity, which is commonly referred to as unintentional doping (UID) and can be significantly enhanced by doping. The unintentional doping of In_2O_3 —with electron concentrations ranging from 10^{17} to 10^{19} cm^{-3} —is typically attributed to hydrogen impurities, such as singly-charged hydrogen interstitials, H_i^+ , and substitutional hydrogen at an oxygen site, H_O^+ .⁵ The origin of the unintentional conductivity of In_2O_3 , has been further associated with oxygen vacancies, V_O^{2+} , acting as doubly-ionized shallow donors. It is still, however, debated whether the V_O are indeed shallow donors^{6–8} or deep donors that do not contribute free electrons.^{5,9} The shallow donor case is also supported by experimental results showing that annealing in oxygen, and thereby removing the oxygen vacancies, decreases the electron concentration in the bulk of In_2O_3 , whereas annealing the material in vacuum does not only restore the electron concentration, but it further increases it.¹⁰ Indium interstitials, that are predicted to act as shallow donors, may also explain these experimental results but are considered unlikely due to their high formation energy.^{8,9} In_2O_3 also possesses a few-nanometers-thick, two-dimensional surface electron accumulation layer (SEAL), the existence of which has been demonstrated by a downward band bending at the surface and the presence of quantized subbands.^{11–13} The conductivity of the SEAL is a particularly important property for applications of In_2O_3 as gas-sensing material¹⁴, facilitates the forma-

tion of ohmic contacts but makes the formation of Schottky contacts challenging.¹⁵ Various methods allow the modulation of the SEAL: A reduction of the SEAL carriers can be achieved by an oxygen plasma treatment of the surface at elevated temperatures^{14,16,17}, by adsorption of oxidizing reactive species, such as O_2 and O_3 ¹⁸ or by intentional compensating acceptor doping.¹⁹ Conversely, annealing treatments^{16,17} or illumination with above-bandgap light^{14,18} can enhance the SEAL. Beyond the unintentional conductivity of In_2O_3 , highly Sn-doped In_2O_3 —commonly known as indium-tin oxide (ITO)^{20–22}—is commercially used as a transparent contact in optoelectronics, such as displays, light-emitting diodes, and solar cells.

Ga_2O_3 , on the other hand, has several polymorphs,²³ the most stable out of which is its β -phase with a monoclinic crystal structure. It has a band gap of approximately 4.8 eV²⁴ and is, thus, transparent within both the visible and well within the UV range. Contrary to In_2O_3 , MBE-grown Ga_2O_3 is insulating at room temperature,²⁵ even though hydrogen has been shown to be a shallow donor in Ga_2O_3 as well.²⁶ As for the nature of V_O , it is widely accepted that they behave as deep donors in Ga_2O_3 . Moreover, Ga_2O_3 typically exhibits upward band bending^{27,28} and, hence, a surface electron depletion layer, providing challenges for the formation of ohmic contacts.²⁹

In theory, a combination of these two compounds can lead to a modulation of their original properties, such as the position in the band gap—and consequently activation energy—of the V_O , the surface electron density or even the presence of the SEAL altogether. Figure 1 (a) graphically illustrates the current knowledge about the relative band-edge positions of cubic In_2O_3 and $\beta\text{-Ga}_2\text{O}_3$, along with the charge state transition levels of V_O with respect to the conduction band minimum (CBM). These have been extrapolated from the formation energy diagrams of Chatratin *et al.*⁸ and Deák *et al.*³⁰, depicted schematically in Fig 1 (b). An increase of the V_O activation energy would be particularly interesting, as it could possibly

benefit the gas sensitivity in In_2O_3 , by reducing both the parallel, parasitic contribution of the bulk conductivity to that of the gas-sensitive surface and the concentration of adsorption centers. A modulation of the SEAL transport properties could also benefit this same application.

Experimentally, a decrease of the Hall electron concentration and mobility of MOCVD-grown $(\text{In}_{1-x}\text{Ga}_x)_2\text{O}_3$ films grown on well-matched $\text{ZrO}_2\text{:Y}$ (YSZ) substrates has been earlier demonstrated by Kong *et al.*³¹ for increasing x up to 0.9. However, limited information is given on the phase purity: the films of this study surprisingly remain cubic up to $x = 0.5$, which contradicts current knowledge about the transition from cubic to monoclinic phase³² and may be explained by a lower incorporation of Ga in the cubic phase than the given total Ga content. Recent investigations by Nagata *et al.*³³ and Swallow *et al.*³⁴ on films grown using pulsed layer deposition (PLD) show the existence of a SEAL up to approximately $x = 0.4$. The latter also demonstrates the lowering of the charge neutrality level with respect to the conduction band minimum from In_2O_3 to InGaO_3 to Ga_2O_3 and, hence, the reduction of the donorlike defects with Ga. However, these studies do not explore the transport properties and, particularly, the electron mobility of those films. Previously, In_2O_3 (and Ga_2O_3) films grown by PLD have been shown to exhibit comparably low electron mobilities,³⁵ likely related to high concentrations of defects.

Another interesting prospect for $(\text{In}_{1-x}\text{Ga}_x)_2\text{O}_3$ alloys for applications requiring transparent conductive materials with a larger band gap than that of ITO can be explored through additional doping with Sn (IGTO). Recent, application-oriented studies towards this direction have demonstrated, for instance, polycrystalline or even amorphous IGTO thin film transistors with high field-effect mobilities.^{36,37} IGTO has been further proposed as an alternative transparent conducting electrode for light-emitting diodes (LEDs), with the intention to increase their external quantum efficiency in the near-ultraviolet spectral range, due to its increased absorption edge, compared to ITO.³⁸

Recently, we have studied well-defined, high-quality, single-crystalline $(\text{In}_{1-x}\text{Ga}_x)_2\text{O}_3$ layers at the low- x end grown by plasma-assisted molecular beam epitaxy (PA-MBE) in terms of surface and film morphology, crystalline quality, and homogeneity⁴⁰ as well as increasing band gap and optical absorption edge with x .⁴¹

In this work we investigate the effect of Ga on the unintentional conductivity of the bulk and the SEAL and demonstrate intentional Sn-doping.

II. EXPERIMENTAL DETAILS

For the purposes of this study, high quality (111)-oriented single-crystalline $(\text{In}_{1-x}\text{Ga}_x)_2\text{O}_3$ films, including one $(\text{In}_{0.92}\text{Ga}_{0.08})_2\text{O}_3\text{:Sn}$ film, were synthesized by PA-MBE on quarters of 2-in. insulating YSZ (111) substrates, whereas full 2-in. insulating Al_2O_3 (0001) (c -plane Al_2O_3) substrates have been employed for the growth of textured samples. The study focuses on the low- x ($x \leq 0.18$) bixbyite phase end of

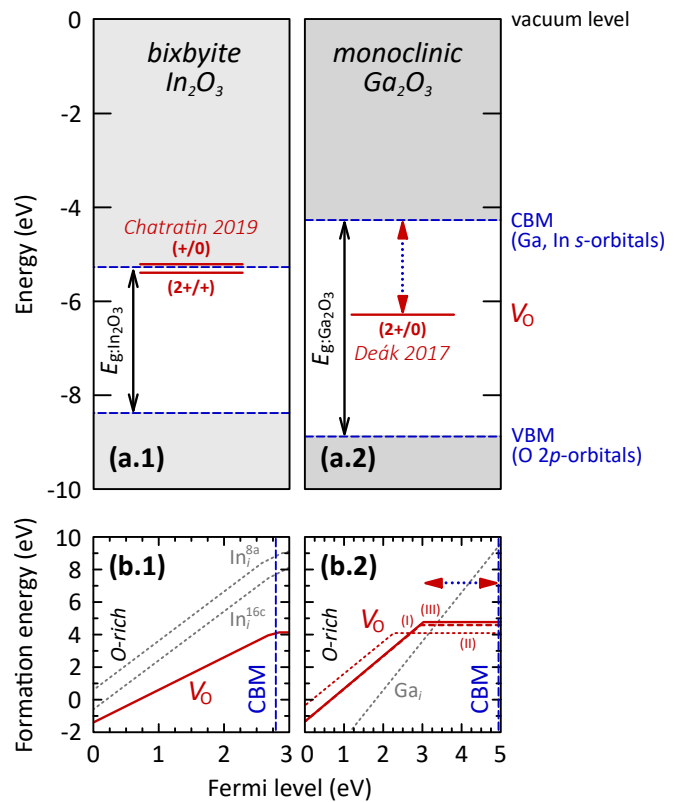


Figure 1. (a) Schematic representation of the band edge and relative oxygen vacancy (V_O) levels of cubic In_2O_3 and β - Ga_2O_3 based on the calculations of Peelaers *et al.*³⁹. (b) Formation energies for donorlike point defects under O-rich conditions. Only the defects with the lowest formation energies and charge state transitions close to the CBM are depicted. These correspond to V_O (red) and metal interstitials (grey), based on the calculations of Chatratin *et al.*⁸ and Deák *et al.*³⁰, respectively. In β - Ga_2O_3 , oxygen and, thus, V_O can be found at three different sites of the unit cell, and the respective formation energies and $(+2/0)$ transition levels are marked with I, II, and III, as in Ref. 8. The dashed blue line corresponds to the CBM at room temperatures.

$(\text{In}_{1-x}\text{Ga}_x)_2\text{O}_3$, hence the substrate choice is based on suitability for heteroepitaxy of pure In_2O_3 . After growth, all samples have been further cleaved into smaller pieces with a size of approximately $5 \times 5 \text{ mm}^2$. The total thickness of the films ranges between 310 nm (SII) and 700 nm [SIII, including the $(\text{In}_{0.92}\text{Ga}_{0.08})_2\text{O}_3\text{:Sn}$ film]. Detailed information on the growth of these single-crystalline samples and the determination of the Ga content therein are reported in our recent work in Ref. 40.

The films on c - Al_2O_3 —not described in our previous work—have been grown under similar conditions upon a pure In_2O_3 buffer layer at the interface. The nucleation of the buffer layer was conducted under an oxygen plasma flux of 2 standard cubic centimeters per minute (SCCM), whereas the main part of the film was grown under a flux of 0.5SCCM. The power of the oxygen plasma source was maintained at 300 W throughout the entire growth procedure. The In-cell temperature was consistently at 850°C for all sam-

ples, corresponding to a beam equivalent pressure (BEP) of 4×10^{-7} mbar. The Ga-containing layers were grown using varying Ga-cell temperatures from 790°C up to 840°C with respective BEPs ranging between $1.1 - 3.5 \times 10^{-8}$ mbar. Under these conditions the films developed with a growth rate of approximately 1 Å/s. The substrate temperature was maintained at 750°C throughout both the nucleation and main film growth—as measured by a thermocouple between the substrate and the substrate heater. This is significantly higher than the substrate temperature used for growth on YSZ, as wetting and overall growth is more straightforward on Al₂O₃. The oxygen flow was discontinued after the completion of the growth from 600°C downwards and the cool-down was essentially realized in vacuum. In contrast to the growth procedure on YSZ, a faster cool-down rate of 0.5°C/s was employed, as there is no concern for film delamination in the case of growth on *c*-Al₂O₃.

Based on the fact that the oxygen chemical potential is higher in an O-rich environment^{8,42} and it decreases with increasing temperature,⁴³ the free electron concentrations of the films have been intentionally varied by annealing treatments in oxygen and vacuum in order to investigate the effect of Ga on transport. Decrease in the electron concentration has been achieved through exposure of the films in an oxidizing environment at high temperature, hereafter referred to as O-annealing. This treatment was performed within a rapid thermal annealing (RTA) system at a final temperature of 800°C at atmospheric pressure for 60 s, excluding the heating and cooling down processing time. Conversely, in order to increase the electron concentration of the films after the initial O-annealing, vacuum annealing treatments were performed. The vacuum annealing was performed in a magnetron sputter system at a background pressure of approximately 5×10^{-7} mbar (which increases up to 10^{-3} mbar upon annealing) for 5 min at a temperature of approximately 500°C. The only exception to this was the Sn-doped film, the vacuum-annealing of which was performed in the growth chamber of the PA-MBE system, under UHV conditions at background pressure around 5×10^{-9} Torr at a substrate temperature of 650°C for a total annealing time of 5 min, excluding the heating and cooling times (ramping rate of 0.25°C/s from and to room temperature, respectively).

Room temperature Hall measurements in the van der Pauw geometry with non-annealed indium contacts in the corners of the samples provided the sheet transport properties, which could be translated into average volume transport properties when combined with the film thickness.

The presence of the SEAL of the films was identified by a combination of conventional soft x-ray photoelectron spectroscopy (SXPES: $h\nu = 1.49$ keV) using an Al K α light source and hard x-ray photoelectron spectroscopy (HAXPES: $h\nu = 5.95$ keV), as also documented in our recent works.^{40,41} HAXPES measurements were performed at room temperature at the revolver undulator beamline at BL15XU of SPring-8.⁴⁴ A detailed description of the experimental setup of HAXPES at the beamline was described elsewhere.⁴⁵ SXPES measurements were performed with a wide acceptance hemispherical electron analyzer combined with a monochroma-

tized Al K α x-ray source (Thermo Scientific, Sigma Probe). A high-resolution hemispherical electron analyzer (VG Scienta R4000) was used to detect the photoelectrons. The total energy resolutions of SXPES and HAXPES were set to 700 meV and 240 meV, respectively. To determine the absolute binding energy, the XPES data were calibrated against the Au 4f_{7/2} peak (84.0 eV) and the Fermi level of Au. Peak fitting of the XPES data was carried out using the Voigt function after subtracting the Shirley-type background.⁴⁶ To investigate the surface band bending behavior, the take-off angle (TOA: θ) dependent PES was performed. TOA is an angle between the normal vector to the sample surface and the detector direction. A high angle PES is surface sensitive, while a low angle it is bulk sensitive. The corresponding inelastic mean free path (IMFP) of HAXPES and SXPES for the In 3d core-level photoemission calculated by the Tanuma–Powell–Penn-2M⁴⁷ are $\lambda_{\text{HAXPES}} = 7.29$ nm and $\lambda_{\text{SXPES}} = 2.39$ nm, respectively, meaning that HAXPES probes three times deeper than SXPES. The probing depth is three times the IMFP,⁴⁸ therefore, our HAXPES measurements probe approximately 22 nm below the sample surface, which can reduce the effect of the surface Fermi level pinning of In₂O₃. To estimate the band bending behaviors of In₂O₃, a detailed XPES spectral analysis was performed using COMPRO (Common Data Processing System) version 11 written by Yoshihara and Yoshikawa, which simulates the potential energy distribution using the convolution of calculated peaks at several TOAs.^{49–51} The simulated spectra were obtained to reproduce the experimental SXPES and HAXPES spectra at several TOAs by adjusting the band bending profiles and minimizing the chi squares of the difference between the simulated and experimental spectra. The band bending direction was denoted as downward and upward, i.e., towards lower and higher binding energies, respectively.

III. RESULTS AND DISCUSSION

Figure 2 shows the transport properties of the single-crystalline and textured films, as determined by four-point Hall effect measurements in the van der Pauw arrangement.

A. Unintentional bulk doping

Electron concentration

The electron concentrations, shown in Fig. 2 (a), on the order of $\sim 10^{17}$ cm⁻³ and $\sim 10^{18}$ cm⁻³ for the pure In₂O₃ films (Ga content $x = 0$) annealed in oxygen and vacuum, respectively, are in good agreement with our previous findings,¹⁰ and confirm, that an oxygen-deficiency provides unintentional shallow donors, e.g., oxygen vacancies. With increasing Ga-content, we observe a slight increase of the electron concentration of the films annealed in oxygen, which may, in principle, be related to impurities in the Ga-source that act as shallow donors in the films.

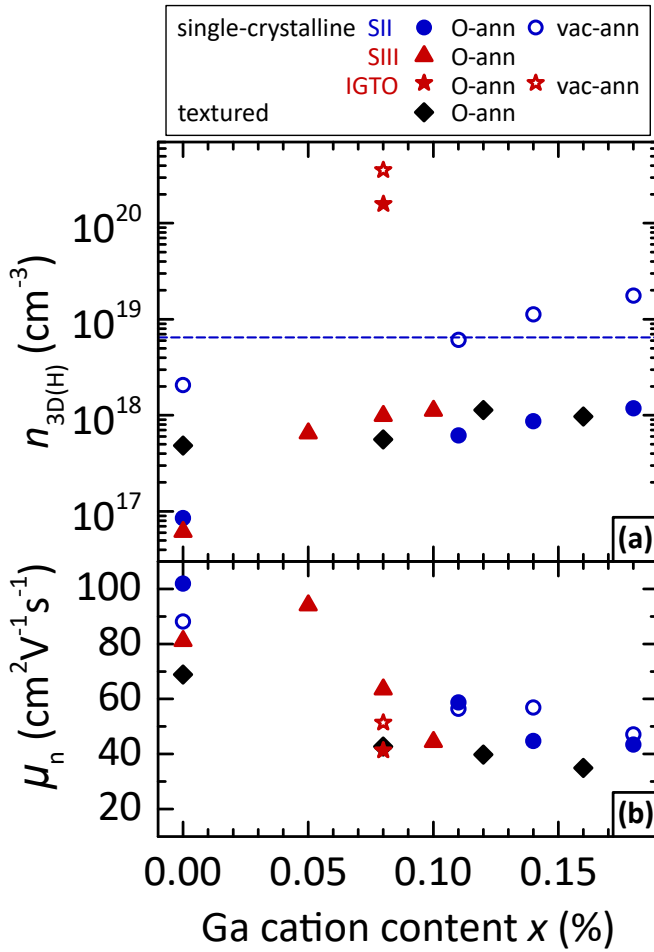


Figure 2. Transport properties of single-crystalline samples on YSZ substrates and textured ones on $c\text{-Al}_2\text{O}_3$: $n_{3D(H)}$ in (a) is the volume electron concentration of the films extracted by dividing the sheet electron concentration from Hall effect measurements by the entire film thickness and μ_n in (b) is the corresponding Hall electron mobility. The samples of series SII and SIII have been grown at different temperatures as described in Ref. 40. Two different states of the films are investigated: oxygen-annealed (O-ann), and vacuum-annealed (vac-ann). The dashed blue line in (a) corresponds to the maximum possible volume electron concentration due to V_O , assuming a charge state transition level as indicated by Ref. 8. The star symbols correspond to an $(\text{In}_{0.92}\text{Ga}_{0.08})_2\text{O}_3:\text{Sn}$ sample (IGTO).

For the single-crystalline films annealed in vacuum, however, the electron concentration is significantly higher and its increase with Ga-content is significantly stronger, which cannot be explained by such impurities and, instead, should be related to point defects due to an oxygen-poor stoichiometry of the films caused by the annealing. A plausible explanation for this unanticipated increase in the Hall electron density $n_{3D(H)}$ could be the formation of donorlike native lattice defects driven by Ga-induced unit cell distortions.

As discussed, it has been shown that the native lattice defects with the lowest formation energy in In_2O_3 that can act as donors are V_O . An O-annealing treatment can potentially fill in V_O in the films and reduce $n_{3D(H)}$. Fig. 2 (a) shows exactly

this effect, if one compares the O-annealed to the vacuum-annealed state of the films. Since the degree of V_O -filling upon O-annealing is not controllable, it is not necessary that the O-annealed Ga-containing samples display a decreased $n_{3D(H)}$ compared to the undoped case. However, assuming the (+/0) transition level for V_O suggested by Chatratin *et al.*⁸ to correspond to the maximum achievable Fermi level in In_2O_3 due to V_O and considering the approximation of the generalized Einstein relation for degenerate and non-degenerate semiconductors of Nilsson⁵², the resulting electron concentration should never exceed $6.5 \times 10^{18} \text{ cm}^{-3}$ [indicated by the horizontal dashed line in Fig. 2 (a)], for an effective electron mass of $0.18 m_e$ as in Ref. 53. All vacuum-annealed Ga-containing samples demonstrate equal or higher $n_{3D(H)}$ than this upper limit. Moreover, the strongly increasing $n_{3D(H)}$ with increasing Ga-content contradicts the expected lowering of the maximum free electron concentration that can be provided by V_O due to their expected decreasing charge transition level with increasing Ga-content.

Unless this charge transition level is significantly higher than theoretically predicted by Chatratin *et al.*⁸, the hypothesis that the $n_{3D(H)}$ increase is due to V_O alone does not suffice and other native donor impurities need to be considered. Those with the next lowest formation energies are metal interstitials acting as triple-donors (In_i^{3+8} , $\text{Ga}_i^{3+26,30,54,55}$). The neutral charge state transition levels for those seem to be well within the conduction band and they, thus, serve as a conceivable explanation for the particularly high electron concentrations observed here. In addition, the smaller ionic size of Ga^{3+} than In^{3+} makes its incorporation as interstitial more likely, which would also be consistent with the increasing electron concentration with increasing Ga-content.

Electron mobility

At a first glance, the trend of decreasing mobility with increasing Ga-content visible in Fig. 2 (b) is not particularly surprising, as mobility is generally expected to decrease with increasing carrier concentration and, thus, ionized impurity concentration. However, in the case of single-crystalline Sn-doped In_2O_3 films, mobility has been reported to be higher than in the single-crystalline films studied here for the same range of electron concentrations ($n_{3D(H)} : \approx 10^{18} - \approx 10^{19} \text{ cm}^{-3}$).⁵⁶ This discrepancy would be consistent with the stronger ionized impurity scattering of doubly-ionized V_O in the $(\text{In,Ga})_2\text{O}_3$ films compared to the singly ionized donors in the Sn-doped In_2O_3 films, theoretically modeled by Preissler *et al.*⁵⁶. This effect is visualized in Fig. 3, with the IGTO data point lying between the $Z = 1$ (Sn^+) and $Z = 2$ (V_O^{2+}). In fact, the good agreement between the experimental data from the vacuum-annealed films and the model curve corresponding doubly-ionized donors implies that the origin of the unexpectedly high electron concentration in the alloy films cannot be attributed—for the most part—to triply-ionized metal interstitials, as suggested previously. This finding indicates that the V_O transition level is indeed significantly higher than theoretically predicted by Chatratin *et al.*⁸. In addition, distortion in

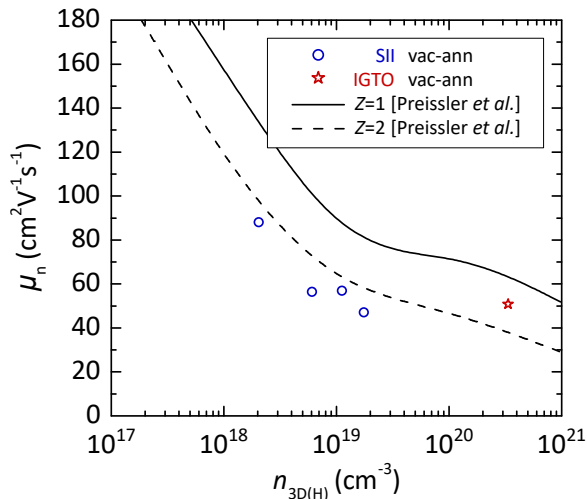


Figure 3. Hall electron mobility, μ_n , as a function of the volume electron concentration from Hall measurements, $n_{3D(H)}$, of the single-crystalline vacuum-annealed samples. The solid and dashed lines correspond to the relation of room temperature Hall mobility to volume electron concentration modeled by Preissler *et al.*⁵⁶ for singly- ($Z = 1$) and doubly-ionized ($Z = 2$) donors, respectively.

the homogeneity of the crystal potential is inevitable in alloys and can limit carrier transport by alloy fluctuation scattering.

Substrate choice does not seem to significantly affect the results in terms of electron concentration. However, decreased mobility is exhibited by the films grown on *c*-Al₂O₃, which happens due to scattering at the grain boundaries of the rotational domains and is not an effect of the Ga incorporation.

B. Intentional bulk doping with Sn

An (In_{0.92}Ga_{0.08})₂O₃:Sn film marked as IGTO in Fig. 2 has been realized as a potential advancement of ITO, with the intention of achieving both comparably high conductivities due to high electron concentrations and an increased band-gap necessary for higher photon energy applications. The enlargement of the band-gap of (In_{1-x}Ga_x)₂O₃ with and without the addition of Sn in comparison to pure In₂O₃ has been confirmed and is discussed in detail in Ref. 41. In this work we investigate its transport properties, which can be directly compared to the (In_{0.92}Ga_{0.08})₂O₃ sample with the same Ga content. As shown in Fig. 2 (a), incorporation of Sn dramatically increases the n_{3D} of the film by more than two orders of magnitude. Doping In₂O₃ and—hence—cubic (In_{1-x}Ga_x)₂O₃ at the low-*x* end—with an Sn⁴⁺ ion should provide one free electron for conduction⁵⁷. The doping effect of Sn in ITO, however, can be largely compensated upon O-annealing treatments, as the ones performed on the films in this study, due to the formation of Sn–oxygen-interstitial clusters, 2Sn_{In}·O_i.⁵⁸ Interstitial oxygen atoms can be removed under reducing conditions, which breaks down those complexes and frees two donors per O_i in the process. Consistent with this defect model, we observed an increase of the electron concentration

from 1.5×10^{20} to 3.3×10^{20} cm⁻³ when comparing the Sn-doped film annealed in oxygen to that annealed in vacuum. Together with the simultaneous increase of electron mobility from 38 to 51 cm²/Vs [shown in Fig. 2 (b)], the film resistivity decreases from 1.1×10^{-3} to 3.7×10^{-4} Ωcm, well into the range typically observed for the regime of ITO, rendering IGTO films a suitable candidate for TCO applications.

C. SEAL presence in the (In_{1-x}Ga_x)₂O₃ films

Magnified SXPES valence band spectra of three representative samples with Ga content of $x = 0.00, 0.11,$ and 0.18 (Fig. 4 (a)) reveal electronic states at the Fermi level (binding energy of 0 eV), indicating the presence of the SEAL. Moreover, In 3*d* core level spectra obtained by SXPES demonstrate a shift towards higher binding energies than those obtained by HAXPES, as compared in Fig. 4 (b). These results suggest a downward band bending at the surface, a necessary precondition for the formation of the SEAL. To identify the degree of the band bending, a detailed spectral analysis using COMPRO has been performed on the In 3*d* spectra obtained by SXPES and HAXPES at various TOA. Fig. 4 (c) shows potential curve at the surface of the pure In₂O₃ film. A drastic potential change has been confirmed within 6 nm from the surface. All alloy films show similar conduction band states around the Fermi level and core level shift, which clearly demonstrates the existence of a SEAL even for samples with Ga cation contents as high as $x = 0.18$.

IV. CONCLUSION

Based on current knowledge on the (+/0) charge transition level of oxygen vacancies in In₂O₃ and Ga₂O₃ and their consequent behavior as shallow and deep donors, respectively, we have anticipated a decrease in unintentional donor concentration upon alloying In₂O₃ with Ga. Nevertheless, the unintentional electron concentration of the (In_{1-x}Ga_x)₂O₃ alloy films is experimentally shown to increase with Ga—particularly for films annealed in vacuum, up to values of 2×10^{19} cm⁻³. Hence, we attribute the increased electron concentration to shallow-donorlike native lattice defects, such as oxygen vacancies or metal—especially Ga—interstitials. According to the reported (+/0) charge transition level of the oxygen vacancy in the band gap of In₂O₃,⁸ this defect cannot be the sole factor contributing to this effect, as in that case we would not observe electron concentrations higher than 6.5×10^{18} cm⁻³. Therefore, either the enhanced carrier concentration is at least partly due to Ga interstitials or unit cell distortion due to Ga-incorporation induces an increased incorporation of oxygen vacancies, whose (+/0) charge transition level is higher than reported in Ref. 8. Moreover, the mobility of the alloy films indicates their conductivity originates from doubly-ionized donors, such as oxygen vacancies, rather than triply-ionized ones, as the metal interstitials. Hence, the theoretically calculated charge level transition of the oxygen vacancies needs to be reconsidered. In addition, the surface elec-

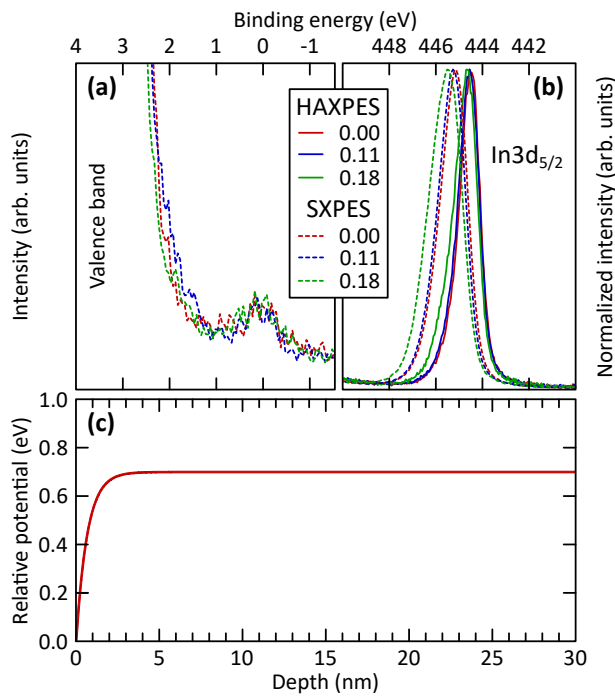


Figure 4. (a) Valence band spectrum from SXPES near the Fermi level (0 eV). (b) In 3d core level spectra of the undoped In_2O_3 , 11 %, and 18 % Ga cation content films obtained by HAXPES (solid line) at TOA of 5° and SXPES (dashed line) at TOA of 9.7° . (c) Potential energy distribution as a function depth estimated by COMPRO. The surface is set at 0 nm.

tron accumulation layer native to In_2O_3 , but not present in Ga_2O_3 , does not seem to be affected by the addition Ga, according to surface-sensitive x-ray photoelectron spectroscopy measurements. Finally, intentional doping of the alloy films with Sn has been demonstrated to result in high electron concentrations up to approximately $3.5 \times 10^{20} \text{ cm}^{-3}$ and mobilities around $50 \text{ cm}^2/\text{Vs}$. This corresponds to an electrical resistivity of $\rho = 3.5 \times 10^{-4} \Omega\text{cm}$, which is comparable to that of pure ITO.

ACKNOWLEDGMENT

We would like to thank Jens Herfort for critically reading this manuscript and Walid Anders for the vacuum annealing processing of the samples. This study was performed in the framework of GraFOx, a Leibniz-ScienceCampus partially funded by the Leibniz association. We are grateful to HiSOR, Hiroshima University, and JAEA/SPring-8 for the development of HAXPES at BL15XU of SPring-8. The HAXPES measurements were performed under the approval of the NIMS Synchrotron X-ray Station (Proposal No. 2018A4601, 2018B4600, and 2019B4602).

REFERENCES

- S. Z. Karazhanov, P. Ravindran, P. Vajeeston, A. Ulyashin, T. G. Finstad, and H. Fjellvåg, *Phys. Rev. B* **76**, 075129 (2007).
- A. Walsh, J. L. F. Da Silva, S.-H. Wei, C. Körber, A. Klein, L. F. J. Piper, A. DeMasi, K. E. Smith, G. Panaccione, P. Torelli, D. J. Payne, A. Bourlange, and R. G. Egdell, *Phys. Rev. Lett.* **100**, 167402 (2008).
- P. D. C. King, T. D. Veal, F. Fuchs, C. Y. Wang, D. J. Payne, A. Bourlange, H. Zhang, G. R. Bell, V. Cimalla, O. Ambacher, R. G. Egdell, F. Bechstedt, and C. F. McConville, *Phys. Rev. B* **79**, 205211 (2009).
- K. Irmscher, M. Naumann, M. Pietsch, Z. Galazka, R. Uecker, T. Schulz, R. Schewski, M. Albrecht, and R. Fornari, *Phys. Status Solidi A* **211**, 54 (2014).
- S. Limpijumngong, P. Reunchan, A. Janotti, and C. G. Van de Walle, *Phys. Rev. B* **80**, 193202 (2009).
- P. Ágoston and K. Albe, *Phys. Rev. B* **84**, 045311 (2011).
- J. Buckeridge, C. R. A. Catlow, M. R. Farrow, A. J. Logsdail, D. O. Scanlon, T. W. Keal, P. Sherwood, S. M. Woodley, A. A. Sokol, and A. Walsh, *Phys. Rev. Materials* **2**, 054604 (2018).
- I. Chatratin, F. P. Sabino, P. Reunchan, S. Limpijumngong, J. B. Varley, C. G. Van de Walle, and A. Janotti, *Phys. Rev. Materials* **3**, 074604 (2019).
- S. Lany and A. Zunger, *Phys. Rev. Lett.* **98**, 045501 (2007).
- O. Bierwagen and J. S. Speck, *Applied Physics Letters* **101**, 102107 (2012).
- P. D. C. King, T. D. Veal, D. J. Payne, A. Bourlange, R. G. Egdell, and C. F. McConville, *Phys. Rev. Lett.* **101**, 116808 (2008).
- K. H. L. Zhang, R. G. Egdell, F. Offi, S. Iacobucci, L. Petaccia, S. Gorovikov, and P. D. C. King, *Phys. Rev. Lett.* **110**, 056803 (2013).
- V. Jovic, S. Moser, A. Papadogianni, R. J. Koch, A. Rossi, C. Jozwiak, A. Bostwick, E. Rotenberg, J. V. Kennedy, O. Bierwagen, and K. E. Smith, *Small* **16**, 1903321 (2019).
- J. Rombach, A. Papadogianni, M. Mischo, V. Cimalla, L. Kirste, O. Ambacher, T. Berthold, S. Krischok, M. Himmerlich, S. Selve, and O. Bierwagen, *Sens. Actuators B* **236**, 909 (2016).
- J. Michel, D. Splith, J. Rombach, A. Papadogianni, T. Berthold, S. Krischok, M. Grundmann, O. Bierwagen, H. von Wenckstern, and M. Himmerlich, *ACS Applied Materials & Interfaces* **11**, 27073 (2019).
- O. Bierwagen, J. S. Speck, T. Nagata, T. Chikyow, Y. Yamashita, H. Yoshikawa, and K. Kobayashi, *Appl. Phys. Lett.* **98**, 172101 (2011).
- T. Berthold, J. Rombach, T. Stauden, V. Polyakov, V. Cimalla, S. Krischok, O. Bierwagen, and M. Himmerlich, *J. Appl. Phys.* **120**, 245301 (2016).
- T. Berthold, S. Katzer, J. Rombach, S. Krischok, O. Bierwagen, and M. Himmerlich, *Physica Status Solidi B: Basic Solid State Physics* **255**, 1700324 (2018).
- A. Papadogianni, J. Rombach, T. Berthold, V. Polyakov, S. Krischok, M. Himmerlich, and O. Bierwagen, *Phys. Rev. B* **102**, 075301 (2020).
- G. S. Chae, *Jpn. J. Appl. Phys.* **40**, 1282 (2001).
- A. N. Tiwari, G. Khrypunov, F. Kurdzesau, D. L. Bätzner, A. Romeo, and H. Zogg, *Prog. Photov.* **12**, 33 (2004).
- M. Y. Tsai, O. Bierwagen, and J. S. Speck, *Thin Solid Films* **605**, 186 (2016).
- R. Roy, V. G. Hill, and E. F. Osborn, *Journal of the American Chemical Society* **74**, 719 (1952).
- T. Matsumoto, M. Aoki, A. Kinoshita, and T. Aono, *Japanese Journal of Applied Physics* **13**, 1578 (1974).
- M. H. Wong, K. Sasaki, A. Kuramata, S. Yamakoshi, and M. Higashiwaki, *Japanese Journal of Applied Physics* **55**, 1202B9 (2016).
- J. B. Varley, J. R. Weber, A. Janotti, and C. G. Van de Walle, *Applied Physics Letters* **97**, 142106 (2010).
- T. C. Lovejoy, R. Chen, X. Zheng, E. G. Villora, K. Shimamura, H. Yoshikawa, Y. Yamashita, S. Ueda, K. Kobayashi, S. T. Dunham, F. S. Ohuchi, and M. A. Olmstead, *Applied Physics Letters* **100**, 181602 (2012).
- A. Navarro-Quezada, Z. Galazka, S. Alamé, D. Skuridina, P. Vogt, and N. Esser, *Applied Surface Science* **349**, 368 (2015).
- S. J. Pearton, J. Yang, P. H. Cary, F. Ren, J. Kim, M. J. Tadjer, and M. A. Mastro, *Applied Physics Reviews* **5**, 011301 (2018).
- P. Deák, Q. Duy Ho, F. Seemann, B. Aradi, M. Lorke, and T. Frauenheim, *Phys. Rev. B* **95**, 075208 (2017).
- L. Kong, J. Ma, F. Yang, C. Luan, and Z. Zhu, *Journal of Alloys and Compounds* **499**, 75 (2010).

- ³²C. Wouters, C. Sutton, L. M. Ghiringhelli, T. Markurt, R. Schewski, A. Hassa, H. von Wenckstern, M. Grundmann, M. Scheffler, and M. Albrecht, *Phys. Rev. Materials* **4**, 125001 (2020).
- ³³T. Nagata, T. Hoga, A. Yamashita, T. Asahi, S. Yagyu, and T. Chikyow, *ACS Combinatorial Science* **22**, 433 (2020).
- ³⁴J. E. N. Swallow, R. G. Palgrave, P. A. E. Murgatroyd, A. Regoutz, M. Lorenz, A. Hassa, M. Grundmann, H. von Wenckstern, J. B. Varley, and T. D. Veal, *ACS Applied Materials & Interfaces* **13**, 2807 (2021).
- ³⁵J. Borgersen, L. Vines, Y. K. Frodason, A. Kuznetsov, H. von Wenckstern, M. Grundmann, M. Allen, J. Zúñiga-Pérez, and K. M. Johansen, *Journal of Physics: Condensed Matter* **32**, 415704 (2020).
- ³⁶B. K. Kim, N. On, C. H. Choi, M. J. Kim, S. Kang, J. H. Lim, and J. K. Jeong, *IEEE Electron Device Letters* **42**, 347 (2021).
- ³⁷D.-H. Kim, H.-S. Cha, H.-S. Jeong, S.-H. Hwang, and H.-I. Kwon, *Electronics* **10**, 1295 (2021).
- ³⁸S. Kim and T. G. Kim, *Thin Solid Films* **591**, 39 (2015).
- ³⁹H. Peelaers, D. Steiauf, J. B. Varley, A. Janotti, and C. G. Van de Walle, *Phys. Rev. B* **92**, 085206 (2015).
- ⁴⁰A. Papadogianni, C. Wouters, R. Schewski, J. Feldl, J. Lähnemann, T. Nagata, E. Kluth, M. Feneberg, R. Goldhahn, M. Ramsteiner, M. Albrecht, and O. Bierwagen, *arXiv:2106.09612* (2021).
- ⁴¹J. Feldl, M. Feneberg, A. Papadogianni, J. Lähnemann, T. Nagata, O. Bierwagen, R. Goldhahn, and M. Ramsteiner, *Applied Physics Letters* **119**, 042101 (2021).
- ⁴²P. Reunchan, X. Zhou, S. Limpijumngong, A. Janotti, and C. G. Van de Walle, *Current Applied Physics* **11**, S296 (2011).
- ⁴³K. Reuter and M. Scheffler, *Phys. Rev. B* **65**, 035406 (2001).
- ⁴⁴S. Ueda, Y. Katsuya, M. Tanaka, H. Yoshikawa, Y. Yamashita, S. Ishimaru, Y. Matsushita, and K. Kobayashi, *AIP Conference Proceedings* **1234**, 403 (2010).
- ⁴⁵S. Ueda, *Journal of Electron Spectroscopy and Related Phenomena* **190**, 235 (2013).
- ⁴⁶D. A. Shirley, *Phys. Rev. B* **5**, 4709 (1972).
- ⁴⁷S. Tanuma, *J. Surf. Sci. Soc. Japan* **27**, 657 (2006).
- ⁴⁸C. Powell, A. Jablonski, I. Tilinin, S. Tanuma, and D. Penn, *Journal of Electron Spectroscopy and Related Phenomena* **98-99**, 1 (1999).
- ⁴⁹<http://www.sasj.jp/compro>.
- ⁵⁰K. Yoshihara, *Journal of Surface Analysis* **13**, 206 (2006).
- ⁵¹M. Imura, S. Tsuda, T. Nagata, H. Takeda, M. Liao, A. Yang, Y. Yamashita, H. Yoshikawa, Y. Koide, K. Kobayashi, T. Yamaguchi, M. Kaneko, N. Uematsu, T. Araki, and Y. Nanishi, *Journal of Applied Physics* **114**, 033505 (2013).
- ⁵²N. G. Nilsson, *physica status solidi (a)* **19**, K75 (1973).
- ⁵³M. Feneberg, J. Nixdorf, C. Lidig, R. Goldhahn, Z. Galazka, O. Bierwagen, and J. S. Speck, *Phys. Rev. B* **93**, 045203 (2016).
- ⁵⁴T. Zacherle, P. C. Schmidt, and M. Martin, *Phys. Rev. B* **87**, 235206 (2013).
- ⁵⁵Z. Hajnal, J. Miró, G. Kiss, F. Réti, P. Deák, R. C. Herndon, and J. M. Kuperberg, *Journal of Applied Physics* **86**, 3792 (1999).
- ⁵⁶N. Preissler, O. Bierwagen, A. T. Ramu, and J. S. Speck, *Phys. Rev. B* **88**, 085305 (2013).
- ⁵⁷Y. Shigesato, S. Takaki, and T. Haranoh, *Journal of Applied Physics* **71**, 3356 (1992).
- ⁵⁸O. Warschkow, L. Miljadic, D. E. Ellis, G. B. González, and T. O. Mason, *Journal of the American Ceramic Society* **89**, 616 (2006).